February 2007

Experimental characterization of the transverse phase space of a 60-MeV electron beam through a compressor chicane

F. Zhou,[1,*] A. Kabel,[2] J. Rosenzweig,[1] R. Agustsson,[1] G. Andonian,[1] D. Cline,[1] A. Murokh,[1] and V. Yakimenko[3]

[1]*Department of Physics and Astronomy, University of California at Los Angeles, Los Angeles, California 90095, USA*
[2]*Accelerator Center, Menlo Park, California 94025, USA*
[3]*Brookhaven National Laboratory, Upton, New York 11973, USA*

Space charge and coherent synchrotron radiation may deteriorate electron beam quality when the beam passes through a magnetic bunch compressor. This paper presents the transverse phase-space tomographic measurements for a compressed beam at 60 MeV, around which energy the first stage of magnetic bunch compression takes place in most advanced linacs. Transverse phase-space bifurcation of a compressed beam is observed at that energy, but the degree of the space charge-induced bifurcation is appreciably lower than the one observed at 12 MeV.

Magnetic bunch compressors are widely used in advanced linacs to shorten the length of electron bunches [1–3]. One of the major challenges for these machines is brightness preservation of the electron beam through magnetic bunch compressors. Space charge, nonlinear correlated energy spread, coherent synchrotron radiation (CSR), and microbunching instability are the main concerns in preserving beam quality through compressors. In order to select a suitable energy for the bunch compression process—in particular for the first stage of compression—two effects must be considered: nonlinear correlated energy spread and space-charge effects. When the compression is chosen at a high energy, the bunch traveling through the linac accumulates too much nonlinear correlated energy spread from the accelerating radio frequency (rf) field. Compressors with nonlinear dependence of path length and energy spread will introduce nonlinear correlated energy spread, giving rise to other nonlinear terms like higher-order dispersion diluting the emittance [4]. When the compression is chosen to take place at a low energy, space-charge effects—which scale with $1/\gamma^2$, where γ is the Lorenz factor—will counteract compression to very short bunches and may also distort 6-dimensional phase-space distribution of the compressed beam. In addition, CSR enhances radiated power loss when the bunch passes through a compressor, which results in severe longitudinal effects, such as energy loss and increase of energy spread. Since these effects occur in a dispersive region, they will eventually create emittance dilution. These detrimental effects had been investigated before [5–8], but the collective parameters measured in these experiments, making *a priori* assumptions on the beam's phase-space distribution, will not represent all information about the beam if the beam's phase space is distorted. More information can be gained if the beam's phase-space distribution is reconstructed using tomographic methods. A group at the University of California at Los Angeles (UCLA) [9] had previously reconstructed the transverse phase-space distribution of a compressed beam with an energy of 12 MeV, using multi-slit diagnostics, and made the first observation of significant phase-space bifurcation. Simulations indicated that the space charge drives the effect. Our present experiment, carried out at the Brookhaven Accelerator Test Facility (ATF), investigates transverse phase-space distribution of a compressed beam with a higher energy of 60 MeV, using quadrupole-scan-based tomography to understand the detrimental effects at an energy close to the one chosen for the first stage of bunch compression in most advanced linacs. Beam parameters and setups for both experiments are compared in Table I.

The tomographic measurements are conducted at the ATF H-line, as schematically shown in Fig. 1. It is composed of a photoinjector, two S-band linac sections, a four-bend chicane, six YAG-screen-based beam-profile-monitors (BPMs), and three triplets for beam focusing. The electrons are produced by a photoinjector whose photocathode is illuminated by a frequency-quadrupled Nd:YAG laser. Two S-band (2856 MHz) linac sections are used to accelerate electrons to a maximum of 72 MeV. A four-bend chicane, designed and manufactured by the UCLA group [10,11], is used to compress bunch length down to below a picosecond (ps) with an appropriately chosen linac's rf phase. Tomography is a technique to reconstruct an object from its projections [12,13]. In its application to beam physics, it is a technique to reconstruct a beam's phase-space distribution. Two classes of tomographic techniques are employed for beam physics applications: multi-slit-based ones [9] for low-energy beams, and quadrupole-scan-based ones [14,15]. The tomography developed at the ATF [15] employs the latter technique: several quadrupoles in the beam transport line are used to rotate the phase-space distribution. For each rotation angle,

*Current address: SLAC, Menlo Park, CA 94025, USA. Electronic address: zhoufeng@slac.stanford.edu

Work supported in part by the US Department of Energy contract DE-AC02-76SF00515

TABLE I. Comparisons of beam parameters and setups for both experiments.

	UCLA previous experiment [9]	Our experiment
Energy (MeV)	12	60
Normalized emittance without compression (μm)	6	2
Beam size in chicane (mm)	1.1	0.2
Tomography technique	Multi-slit	Quad-scan
Fully compressed bunch length	Sub-ps	Sub-ps
Charge (nC)	0.25	0.2

the image of the beam on the YAG screen (taken, for example, by a CCD camera) represents a two-dimensional projection of the original four-dimensional transverse phase spaces of the electron beam. Projections of the electron beam taken at various phase advances can be used to infer the phase-space density distribution. The phase-space reconstruction technique uses the "filtered back-projection" [13]. The desired density in phase space x-x', $\mu(x, x')$, is obtained from the measured data $\lambda_\phi(x)$ by the following algorithm; $\lambda_\phi(x)$ can be obtained from the BPM data by projecting the x-y distribution onto the x-axis for a given phase advance, ϕ. Total rotation angle is 180°. The phase-space density distribution $\mu(x, x')$ is given by the following integral of the "filtered projection":

$$\mu(x, x') = \int_0^\pi \lambda_\phi{}^+(\xi) d\phi \Big|_{\xi = x\cos\phi + x'\sin\phi}, \qquad (1)$$

where $\lambda_\phi{}^+(\xi)$ is called as the "filtered projection," which is obtained from the projection data $\lambda_\phi(x)$ by the following equation:

$$\lambda_\phi{}^+(ms) = \frac{1}{4s}\lambda_\phi(ms) - \frac{1}{\pi^2 s} \sum_{\substack{n \\ (m-n)\text{odd}}} \frac{\lambda_\phi(ms)}{(m-n)^2}, \qquad (2)$$

where m is an integer, s is the pixel size, and $x = ms$. Phase-space distribution in the y-plane can be obtained in the same manner. The resolution of the reconstructed transverse phase space was extensively studied; it was concluded that 32 projections in total were required to achieve a sufficiently high resolution [15].

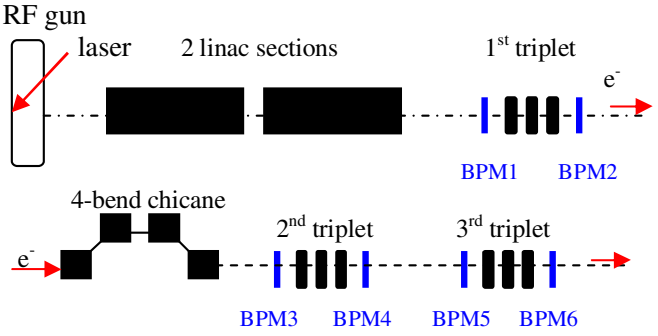

FIG. 1. (Color) Schematic layout of the ATF H-line; the beam bends in the vertical (y) plane in the chicane.

In the experiment, two triplets downstream of the chicane shown in Fig. 1 are used to match the beam optics for different phase rotations. The Twiss parameters inside the chicane and at the chicane exit are measured. The former is directly related to the space-charge effects, while the latter are taken as initial Twiss parameters for optics of different phase rotations. A Mathcad-based program [16] is developed to obtain the Twiss parameters at each location by measuring beam spot sizes at the BPMs along the H-line [17]. It shows that vertical beam spot sizes σ_y at the third and fourth dipoles are smaller than 200 μm rms without time-energy correlation. The Twiss parameters with different time-energy correlations at the chicane exit are also measured.

A conventional magnetic bunch compressor consists of two elements: a linac as an energy modulator, and a non-isochronously achromatic section (e.g., chicane). At the ATF two S-band linac sections provide a time-energy correlation along the bunch length by moving the rf phase off-crest. The induced energy spread is expressed in terms of parameters φ, $\Delta\varphi$, δ_0, E_0, E, and k, where φ is the off-crest rf phase, $\Delta\varphi$ is the bunch length in units of rf wavelength, δ_0 is the initial energy spread, and E_0 is the initial beam energy. The final energy $E \sim E_0 + eV_{\text{rf}}\cos(kz + \varphi)$, e is the electron charge, V_{rf} is the accelerating voltage, and k is the rf wave number. As the chicane is nonisochronous, it has an energy-dependent path length, expressed, to the first order, by its momentum compaction matrix element R_{56}. After passing through the chicane, the final rms bunch length downstream of the chicane is expressed in terms of parameters κ, R_{56}, σ_{z0}, $\sigma_{\delta 0}$, E_0, and E [18], where $\kappa = \partial\delta/\partial z$ is the energy "chirp" with longitudinal position, $\sigma_{\delta 0}$ is the initial rms energy spread, and σ_{z0} is the initial rms bunch length. Proper tuning of the linac's rf phase to impart the required energy spread along the bunch results in compression as the bunch propagates along the chicane. In our case, the R_{56} of the chicane is 8.9 cm when the dipole bending angle is 20°. Simulations with ELEGANT code [19] predict that the initial 1 ps rms bunch length can be compressed down to 100 fs rms with ~0.32% rms of correlated energy spread.

The phenomena that the space-charge and/or CSR effects will severely distort the energy spectrum of, and

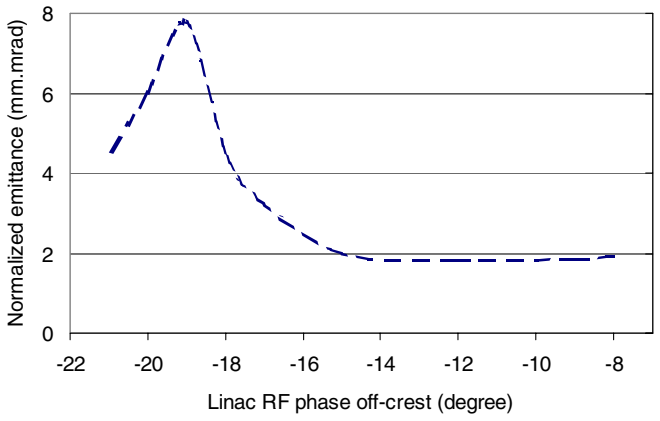

FIG. 2. (Color) Measured normalized transverse emittance vs linac's rf off-crest phase (note that the minimum energy spread was achieved at the linac's rf off-crest phase of $-8°$).

induce emittance growth on, the compressed beam [20,21] are used to determine the compression degree. In our measurements, the energy spectrum is severely bifurcated at $-19°$ of rf off-crest. The minimum energy spread is obtained at $-8°$ of off-crest rf instead of on-crest due to the wakefield and longitudinal space-charge effects. The normalized emittance is measured as a function of the linac's rf off-crest phase by monitoring beam spot sizes at four BPMs downstream of the chicane. Figure 2 shows that the emittance is increased from $\sim$2 to 8 μm at $-19°$ of rf off-crest at a beam charge of 200 pC. The emittance growth reasonably agrees with ELEGANT code simulations. Both the energy spectrum and emittance data indicate that the bunch is close to the full compression at $-19°$ of rf off-crest from both linac sections.

The phase-space tomographic measurements are focused on a compressed beam at 60 MeV. A lower rf-gun's rf phase is chosen [22–24] during the measurements so that the bunch length at the linac exit is shorter, taking advantage of the bunching in the rf-gun. It turns out the smaller correlated energy spread is helpful in achieving compression, and results in smaller chromatic effects downstream of the chicane. Procedures used to obtain the transverse phase-space distributions of a beam consist of four steps: (i) measure the Twiss parameters at the chicane exit for the beams without compression, under, near full, full, and over compression; (ii) match the beam optics with both the second and third triplets for different phase rotations, based on the measured Twiss parameters at the chicane exit; (iii) record beam images at the BPM6 using phase advances for different phase rotations; and (iv) reconstruct the transverse phase space using the "filtered projection" as described in Eqs. (1) and (2). Figure 3 shows typical reconstructed transverse phase spaces of an uncompressed beam at the minimum energy spread (rf phase off-crest by $-8°$), and beams with under, near full, full, and over compression at the linac's rf phase off-crest by $-14°$, $-18°$, $-19°$, and $-22°$, respectively. All measurements are conducted at a beam charge of 200 pC. The images show that the phase-space distributions are not bifurcated in the nonbending (x) plane for all compression values used, and that the distributions are reasonably similar. The phase-space distributions in the bending (y) plane are expanded significantly and also exhibit a slight bifurcation at near full compression ($-18°$). At full compression ($-19°$), it is bifurcated notably, but not as pronouncedly as observed at 12 MeV. The observed beam spot sizes in the third and fourth bend are smaller than 200 μm rms. When the beam spot sizes in the chicane are adjusted to slightly larger values, no phase-space bifurcation could be observed. This is attributed to the reduced space charge by enlarging beam size. For both under and over compression, the phase spaces are dramatically shrunk in comparison to the one at full compression.

Simulations with ELEGANT code including CSR effects, but without space-charge effects, do not display any bifurcation. We can assume that transverse phase-space expansion of the compressed beam is primarily caused by the

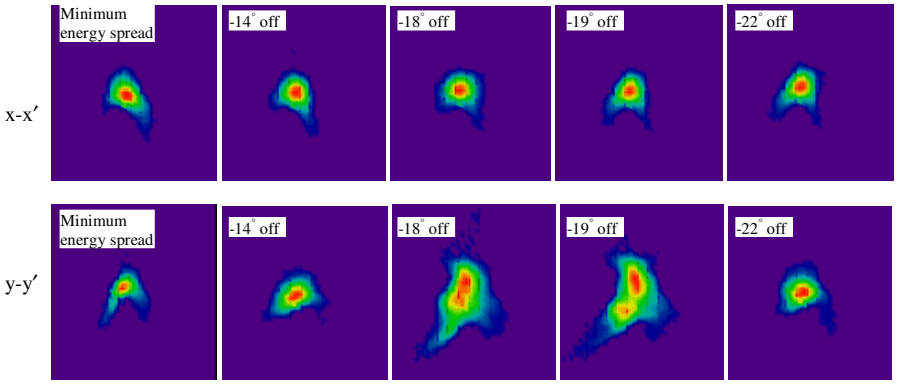

FIG. 3. (Color) Reconstructed transverse phase spaces of 60 MeV beams with minimum energy spread, under, near full, full, and over compression operating at $-8°$, $-14°$, $-18°$, $-19°$, and $-22°$ rf off-crest phase, respectively; top plots are x-x' (nonbending plane), and bottom plots are y-y' (bending plane); the abscissa axis is x (y), and the ordinate axis is x' (y'). The calibration in all sets is 3.2 mm $\times$ 0.71 mrad.

CSR effects. For further investigations, TRAFIC4 [25,26], which includes both CSR and space-charge effects, is used to simulate the compressor chicane. In this code, the bunch is represented by a set of macroparticles. Each of the three-dimensional macroparticles has a longitudinal and transverse size, thus obtaining a smooth charge distribution. Their electromagnetic fields are calculated from first principles by numerically solving Maxwell's equations, correctly considering all retardation effects. The particles are tracked self-consistently, storing away their history in the process, which needs to be considered for future calculations of retarded fields. We use the code to track several thousand macroparticles through the chicane. The initial conditions, such as Twiss parameters, beam energy, etc., are taken from experimental data. Figure 4 shows the simulated transverse phase space in the bending plane for fully compressed (a) and overcompressed (b) beams, respectively. It shows the two humps are distinctly separated in the beam with full compression while the humps are less distinctly separated at over compression. These simulations qualitatively agree with the phenomena observed in the experiment. Simulations using TRAFIC4 (both space-charge and CSR effects) combined with ones using ELEGANT (CSR effects) may indicate that space-charge effects play the dominant role in the transverse bifurcation. In comparison to Ref. [9], the longitudinal space-charge field in our experiment is reduced by a factor of 25, and thus the force creating bifurcation should be drastically mitigated at the higher energy.

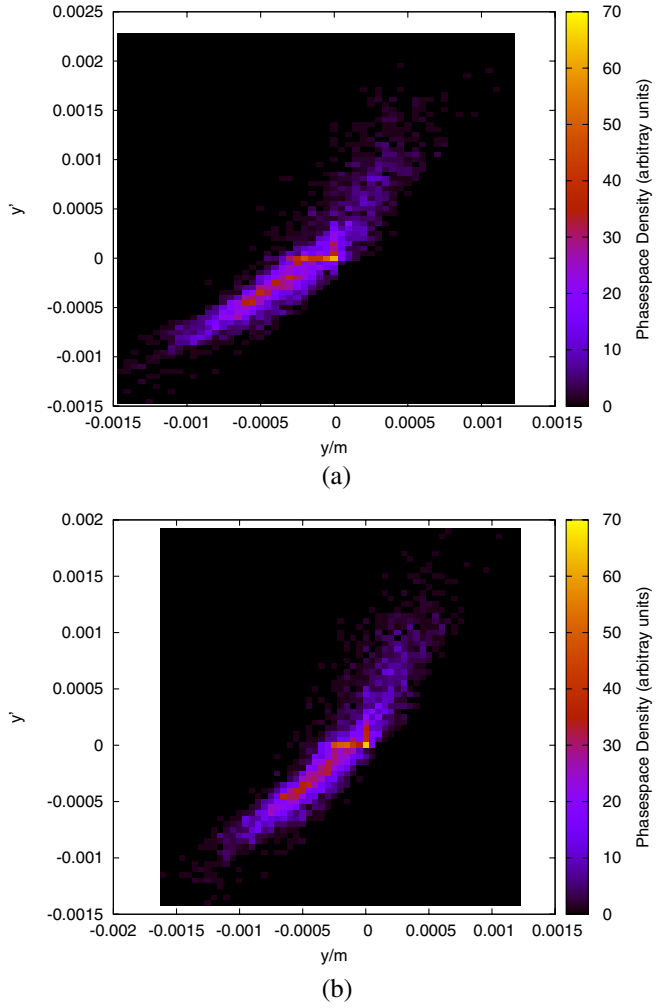

FIG. 4. (Color) TRAFIC4 simulation results for transverse phase-space distributions in the bending plane for fully compressed (a) and overcompressed beams (b); units of y' are arbitrary, and the vertical coordinate is the phase-space density (arbitrary units). Also displayed are the phase-space isopycnics, clearly exhibiting the bifurcation in the fully compressed case.

In summary, the transverse phase-space distributions of 60 MeV beams through a compressor chicane are measured using quadrupole-scan-based tomography. The reconstructed transverse phase-space distributions for different degrees of bunch compressions are essentially constant in the nonbending plane. The ones of a fully compressed beam in the bending plane are significantly increased in phase-space volume, as well as bifurcated, but notably less than previously observed at an energy of 12 MeV. The phase-space distributions' volumes in both the undercompressed and overcompressed cases are significantly smaller than at full compression. The experimental data, in conjunction with simulations using the TRAFIC4 and ELEGANT codes, indicates that: (i) the space-charge force drives the phase-space bifurcation; (ii) the phase-space volume increases are primarily caused by CSR effects; (iii) the space-charge forces driving the bifurcation are significantly mitigated at 60 MeV. These results may be helpful to suitably select the energy of the first stage of bunch compressions at advanced linacs.

ACKNOWLEDGMENTS

Feng Zhou thanks Dr. I. Ben-Zvi for his ongoing support and encouragement, and also acknowledges the technical support from the ATF staff. This work was supported by Office of Sciences, U.S. Department of Energy.

[1] International study group progress report on linear collider development, SLAC-R-559, SLAC, Stanford, USA, 2000.
[2] TESLA technical design report, DESY 2001-011, DESY, Hamburg, Germany, 2001.
[3] LCLS design report, SLAC-R-593, SLAC, Stanford, USA, 2002.
[4] A VUV Free Electron Laser at the TESLA Test Facility at DESY, Conceptual Design Report, TESLA-FEL 95-03, DESY, Hamburg, Germany, 1995.
[5] H. Braun, F. Chautard, R. Corsini, T. Raubenheimer, and P. Tenebaum, Phys. Rev. Lett. **84**, 658 (2000).
[6] H. Braun, R. Corsini, L. Groening, F. Zhou, A. Kabel, T. Raubenheimer, R. Li, and T. Limberg, Phys. Rev. ST Accel. Beams **3**, 124402 (2000).

[7] M. Borland and J. W. Lewellen, in *Proceedings of the 2001 Particle Accelerator Conference, Portland* (IEEE, Piscataway, 2001).

[8] W. Graves, G. Carr, L. DiMauro, A. Doyuran, R. Heese, E. Johnson, C. Neuman, G. Rakowsky, J. Rose, J. Rudati, T. Shaftan, B. Sheehy, J. Skaritka, L.-H. Yu, and D. Dowell, in *Proceedings of the 2001 Particle Accelerator Conference, Chicago* (IEEE, Piscataway, 2001).

[9] S. Anderson, J. Rosenzweig, P. Musumeci, and M. Thompson, Phys. Rev. Lett. **91**, 074803 (2003).

[10] R. Agustsson, Master's thesis, UCLA, Los Angeles, 2004, http://pbpl.physics.ucla.edu/Literature/_library/agustsson_2004_606.pdf.

[11] J. Rosenzweig, ATF users Meeting, BNL, 2004, http://www.bnl.gov/atf/Meetings/ATF2004/Default.htm.

[12] P. Gilbert, J. Theor. Biol. **36**, 105 (1972).

[13] W. Swindell and S. Webb, in *The Physics of Medical Imaging*, edited by S. Webb (IOP, London, 1992), pp. 98–127.

[14] C. B. McKee, P. G. O'Shea and J. M. J. Madey, Nucl. Instrum. Methods Phys. Res., Sect. A **358**, 264 (1995).

[15] V. Yakimenko, M. Babzien, I. Ben-Zvi, R. Malone, and X.-J. Wang, Phys. Rev. ST Accel. Beams **6**, 122801 (2003).

[16] Mathcad Users' guide, Mathsoft Inc., Cambridge, USA, 2000, http://www.mathsoft.com/.

[17] F. Zhou, R. Agusstson, G. Andonian, D. Cline, A. Murokh, J. Rosenzweig, I. Ben-Zvi, and V. Yakimnko, in *Proceedings of the 2005 Particle Accelerator Conference, Knoxville* (IEEE, Piscataway, 2005).

[18] P. Emma, in Proceedings of the Workshop on Future Light Sources, ANL, 1999, http://www.aps.anl.gov/conferences/FLSworkshop/proceedings/TOC.html.

[19] M. Borland, Technical Report No. LS-287, ANL, 2000.

[20] P. Piot, BNL-52624, Brookhaven National Laboratory, 2001.

[21] A. Murokh, ATF/BNL News Letter, BNL, 2005, http://www.bnl.gov/atf/Weekly_Reports/reports.html.

[22] X. Wang, X. Qiu, and I. Ben-Zvi, Phys. Rev. E **54**, R3121 (1996).

[23] F. Zhou, I. Ben-Zvi, M. Babzien, X. Y. Chang, A. Doyuran, R. Malone, X. J. Wang, and V. Yakimenko, Phys. Rev. ST Accel. Beams **5**, 094203 (2002).

[24] F. Zhou, J. H. Wu, M. Babzien, I. Ben-Zvi, J. Murphy, X. J. Wang, M. Woodle, and V. Yakimenko, Phys. Rev. Lett. **89**, 174801 (2002).

[25] A. Kabel, M. Dohlus, and T. Limberg, Nucl. Instrum. Methods Phys. Res., Sect. A **455**, 185 (2000).

[26] A. Kabel, Y. Cai, M. Dohlus, T. Sen, and R. Uplenchwar, Nucl. Instrum. Methods Phys. Res., Sect. A **557**, 189 (2006).